

This Supplementary Information replaces the original version published on 16 January 2026. The files previously available on the platform are now accessible from the repository at <https://zenodo.org/records/18154388>.

SUPPORTING INFORMATION FOR THE WORK

The Methanol Electrooxidation Activity and the CO-Resilient Surface of a $\text{La}_x\text{Fe}_{1-y-z}\text{Cu}_y\text{Pd}_z\text{O}_3$ Perovskite

Manuel Antuch,^{*a} Madjid Tarabet,^b Rubén Parra,^c Carmen Ciotonea,^d Alicia D. García,^c Luis F. Desdin-García,^e Mukaddar Sk,^f Ranjit Thapa,^{f,g} Sébastien Royer^{d*}

^a *Univ. Lille, CNRS, Centrale Lille, Univ. Artois, UMR 8181, UCCS, Unité de Catalyse et Chimie du Solide, Lille F-59000, France.*

^b *Horiba France SAS, 455 Avenue Eugène Avinée, 59120, Loos, France*

^c *Laboratorio de Bioinorgánica, Departamento de Química General e Inorgánica, Facultad de Química, Universidad de La Habana, La Habana, C.P. 10400, Cuba.*

^d *Université du Littoral Côte d'Opale, UCEIV UR 4492, Maison de Recherche en Environnement Industriel 1, 145 Avenue Maurice Schumann 59140 Dunkerque, France.*

^e *Centro de Aplicaciones Tecnológicas y Desarrollo Nuclear (CEADEN), Miramar C.P. 11300, La Habana, Cuba.*

^f *Department of Physics, SRM University AP, Amaravati 522240, Andhra Pradesh, India.*

^g *Centre for Computational and Integrative Sciences, SRM University – AP, Amaravati 522240, Andhra Pradesh, India.*

Corresponding authors:

Manuel Antuch manuel.antuch@centralelille.fr

Sébastien Royer sebastien.royer@eilco.univ-littoral.fr

This Supplementary Information replaces the original version published on 16 January 2026. The files previously available on the platform are now accessible from the repository at <https://zenodo.org/records/18154388>.

1. Additional microscopy characterization

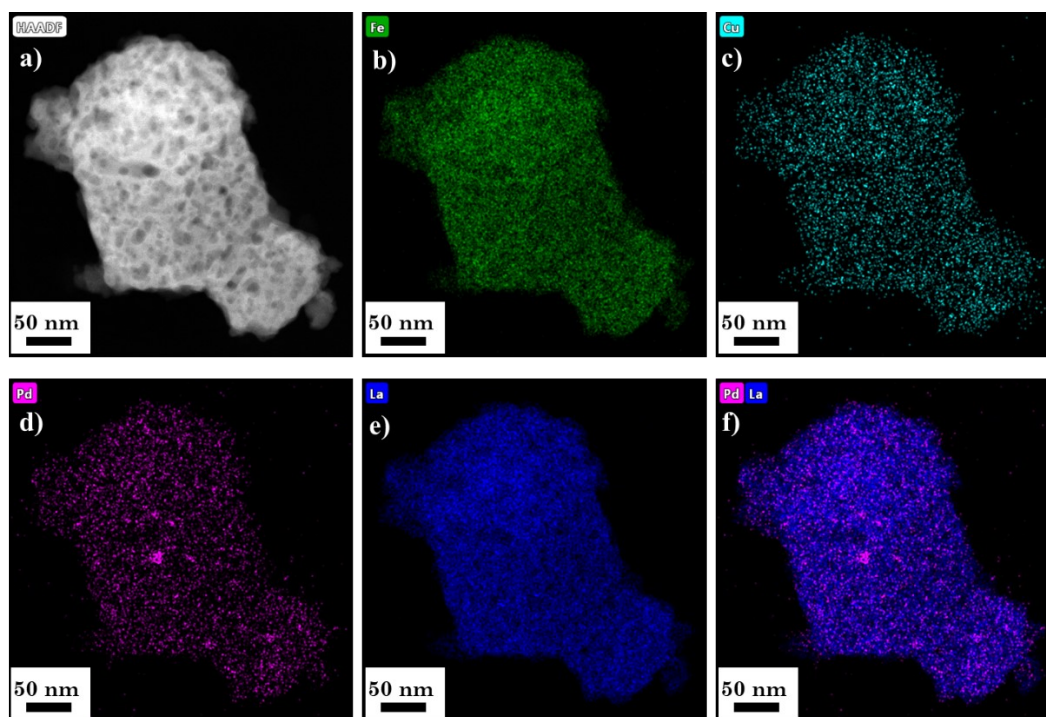


Figure S1 a) high-angle annular dark-field scanning transmission electron microscopy (HAADF) of the $\text{La}_{0.88}\text{Fe}_{0.93}\text{Cu}_{0.05}\text{Pd}_{0.02}\text{O}_3$ perovskite; b) elemental mapping of Fe; c) elemental mapping of Cu; d) elemental mapping of Pd; e) elemental mapping of La; f) superimposition of the elemental mapping of Pd and La.

This Supplementary Information replaces the original version published on 16 January 2026. The files previously available on the platform are now accessible from the repository at <https://zenodo.org/records/18154388>.

2. Additional XPS data

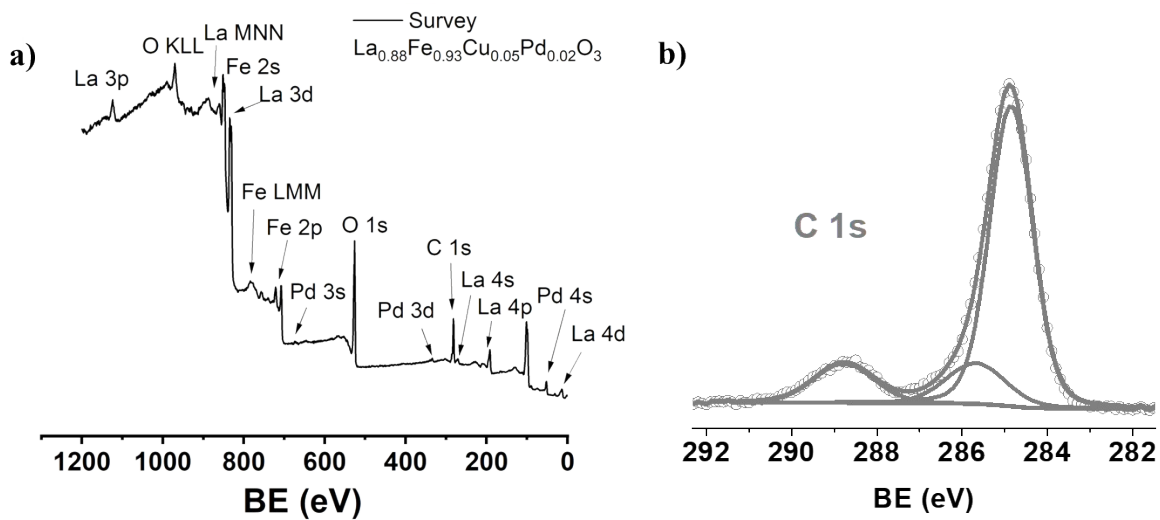


Figure S2. (a) XPS survey spectrum and (b) narrow scan of the C 1s core level.

This Supplementary Information replaces the original version published on 16 January 2026. The files previously available on the platform are now accessible from the repository at <https://zenodo.org/records/18154388>.

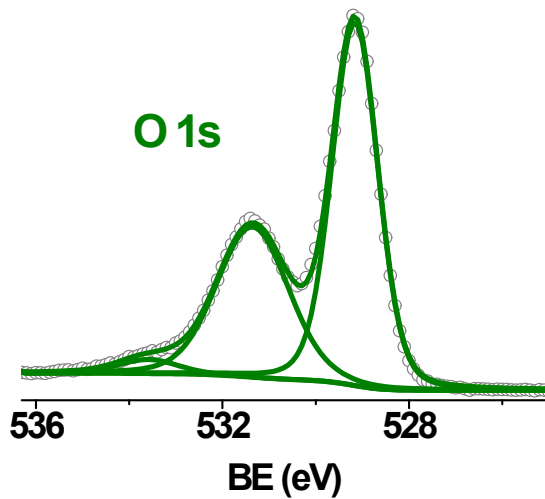


Figure S3. XPS narrow scan of the O 1s core level.

This Supplementary Information replaces the original version published on 16 January 2026. The files previously available on the platform are now accessible from the repository at <https://zenodo.org/records/18154388>.

Table S1. Semiquantitative determination of elements by XPS.

Atomic percent (%)	
O	65.80
La	17.91
Fe	14.59
Cu	1.29
Pd	0.41
La + Fe + Cu + Pd	34.20
Fe + Cu + Pd	16.29
Ratios	
La / (Fe + Cu + Pd)	1.10
Fe / (Fe + Cu + Pd)	0.90
Cu / (Fe + Cu + Pd)	0.08
Pd / (Fe + Cu + Pd)	0.03
O / La	3.67
La / Fe	1.23
Cu/Pd	3.15
Cu/Fe	0.09
Pd/Fe	0.03

This Supplementary Information replaces the original version published on 16 January 2026. The files previously available on the platform are now accessible from the repository at <https://zenodo.org/records/18154388>.

3. Oxygen Evolution Reaction at $\text{La}_{0.88}\text{Fe}_{0.93}\text{Cu}_{0.05}\text{Pd}_{0.02}\text{O}_3$ electrodes

Concerning the OER, microkinetic analysis has been proposed based on the mechanism S1 (equations S1 to S3). Based on these equations, dual Tafel slopes are observed when equation S3 represents the rds and certain conditions for the coverage of intermediates are met, i.e., when θ_{OH} and $\theta_O \approx 0$, simulation a 30 mV/dec is predicted, while when $\theta_{OH} \approx 1$ and $\theta_O \approx 0$, a 60 mV/dec slope should appear. On the other hand, 40 mV/dec slope appears when reaction S2 is the rds. Finally, 120 mV/dec slope exists when reaction S1 is the rds.

Mechanism S1



In this particular case, the experimental Tafel slope was 104 mV/dec, which is close to 120 mV/dec, thus suggesting that the initial water discharge to form the OH- intermediate is the rds for this transformation. Other Tafel slopes for similar systems are summarized in Table S2.

This Supplementary Information replaces the original version published on 16 January 2026. The files previously available on the platform are now accessible from the repository at <https://zenodo.org/records/18154388>.

Table S2. Succinct compendium of Tafel slopes for the HER and the OER at various materials.

Material	Tafel slope	Conditions	Reference
$\text{LnBaCo}_2\text{O}_{5+\delta}$ *	60		[1]
NiCo_2O_4 (nanoneedle)	292	KOH 1 M	[2]
NiCo_2O_4 (nanosheet)	393		
SrVO_3	235	NaOH 1 M	[3]
LaCoO_3	70 (low η)		
	135 (high η)		

* Ln = Pr, Sm, Gd, Ho.

This Supplementary Information replaces the original version published on 16 January 2026. The files previously available on the platform are now accessible from the repository at <https://zenodo.org/records/18154388>.

4. Benchmark comparison of mass activities of MeOH electrocatalysts

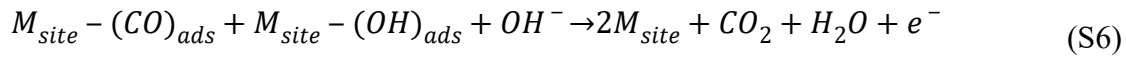
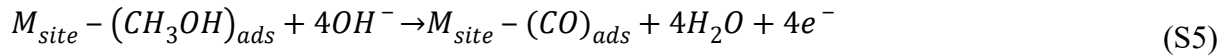
Table S3. Comparison of mass activities for different MeOH electrocatalysts.

Material	Mass activity	Reference
$\text{La}_{0.88}\text{Fe}_{0.93}\text{Cu}_{0.05}\text{Pd}_{0.02}\text{O}_3$	1041 mA / mg	This work
Pt/C	441 mA / mg-Pt	[4]
Pt/RuO ₂	6766 mA / mg-Pt	[4]
Pt ₇ Zn/carbon cloth	5890 mA / mg-Pt	[5]
Pt ₄ Zn/carbon cloth	3920 mA mg-Pt	[5]
Pt ₉ Zn/carbon cloth	2530 mA / mg-Pt	[5]
Pt/carbon cloth	1490 mA / mg-Pt	[5]
Pt–Pd catalyst	2235.4 mA / mg-metals	[6]
Pt–Pt	1124.1 mA / mg-metals	[6]
Pd–Pd	837.7 mA / mg-metals	[6]
single-nickel-atom-alloyed platinum hexagonal nanocrystals/porous graphdiyne (NiPtSAA/GDY)	4400 mA / mg-(Pt+Ni)	[7]
3.5% Pt/mesoporous-WC	1851 mA/mg-Pt	[8]
PtNT	88 mA / mg	[9]
Rh ₂ P-Pt/C	460 mA / mg-noble metal	[10]
Pt ₃ Rh nanoclusters	1392.5 mA / mg	[11]
Co ₈₈ Pt ₆ Ru ₆ /NC	280 mA / mg-Pt+Ru	[12]
Pt(10%)–Au hollow nanourchin (HNU)	0.80 mA / μg-Pt	[13]
Nanoporous palladium (NPPd)	262 mA / mg	[14]
Pt ₃ Te ₆ Co ₂ NRs/C	1470 mA / mg-Pt	[15]
Pt ₅₂ Fe ₁₁ Co ₁₀ Ni ₁₁ Cu ₁₀ Ag ₈	462–504 mA / mg	[16]
PtCo nanocrosses	692 mA / mg-Pt	[17]
PtRuCu/C	1350 mA / mg-Pt	[18]
Pt NPs	70.1 mA / mg	[19]
Pt NFs	87.7 mA / mg	[19]
bimetallic PtRu catalyst supported on carbon black (20 wt% Pt, 10 wt% Ru, Johnson Matthey)	400 mA / mg-Pt	[20]
CeOx/PtCu/Ce- CuOx/C	332.5 mA / mg-Pt	[21]
Cubic core shell Pd@Pt	580 mA / mg-Pt	[22]
Pd–Cu (3:1) nanoalloy	659.4 mA / mg	[23]
PdAg/C	172 mA / mg-Pd	[24]

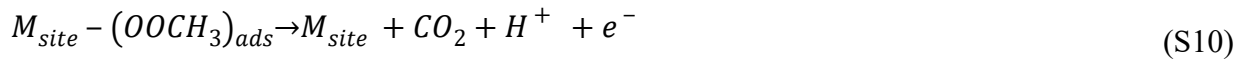
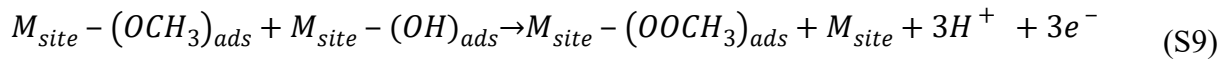
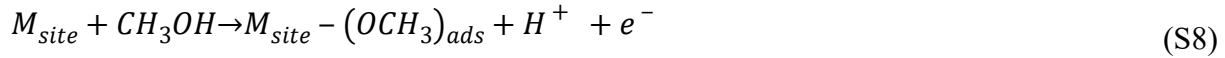
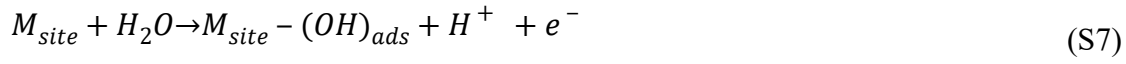
This Supplementary Information replaces the original version published on 16 January 2026. The files previously available on the platform are now accessible from the repository at <https://zenodo.org/records/18154388>.

5. Alternative mechanisms for the methanol oxidation reaction

Mechanism S2[25,26]



Mechanism S3[27]



Concerning mechanism S3, equation 1 describes the adsorption and discharge of OH^{-} ions, while equation 2 sums up complex steps leading to the production of $(CO)_{ads}$ and finally equation 3 shows the interfacial reaction between key intermediates $(CO)_{ads} + (OH^{-})_{ads}$ to leave the M_{site} regenerated. On the other hand, the first step in mechanism S4 (equation 4) is analogous to equation 1. Equation 5 describes methanol discharge to produce adsorbed methoxy moieties, that react with adsorbed hydroxyl through the process shown in equation 6, to yield CO_2 via equation 7 and the release of active M_{site} .

This Supplementary Information replaces the original version published on 16 January 2026. The files previously available on the platform are now accessible from the repository at <https://zenodo.org/records/18154388>.

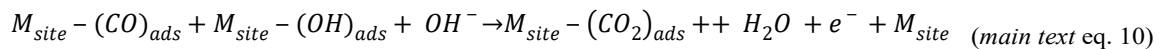
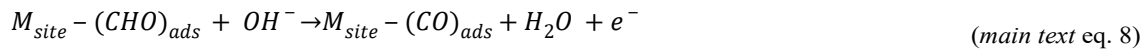
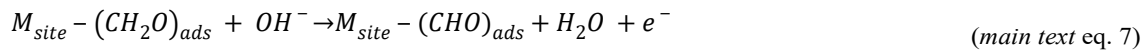
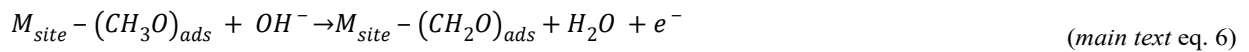
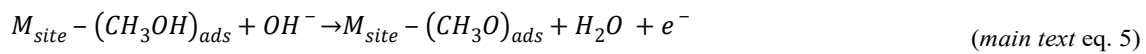
This Supplementary Information replaces the original version published on 16 January 2026. The files previously available on the platform are now accessible from the repository at <https://zenodo.org/records/18154388>.

6. Parameters of the multistep methanol oxidation reaction

Table S4. Mechanistic parameters corresponding to equations 4-11, for the specific cases where different steps described each equation is the rate determining, assuming the transfer coefficient $\alpha = 0.5$. [28]

Rate determining step*	γ	ν	r	α_{eff}	Expected $\frac{\partial \eta}{\partial \log i}$ (mV / dec)
Equation 4	0	1	0	0	-
Equation 5	0	1	1	0.5	118
Equation 6	1	1	1	1.5	39
Equation 7	2	1	1	2.5	24
Equation 8	3	1	1	3.5	17
Equation 9	4	1	1	4.5	13
Equation 10	5	1	1	5.5	11
Equation 11	6	1	0	6	10

*The numbering of the equations in this column corresponds to the numbering of equations in the main manuscript, which is reproduced here with identical numbering as in the main text, for the sake of simplicity.



This Supplementary Information replaces the original version published on 16 January 2026. The files previously available on the platform are now accessible from the repository at <https://zenodo.org/records/18154388>.

This Supplementary Information replaces the original version published on 16 January 2026. The files previously available on the platform are now accessible from the repository at <https://zenodo.org/records/18154388>.

7. Additional electrochemical data for methanol oxidation

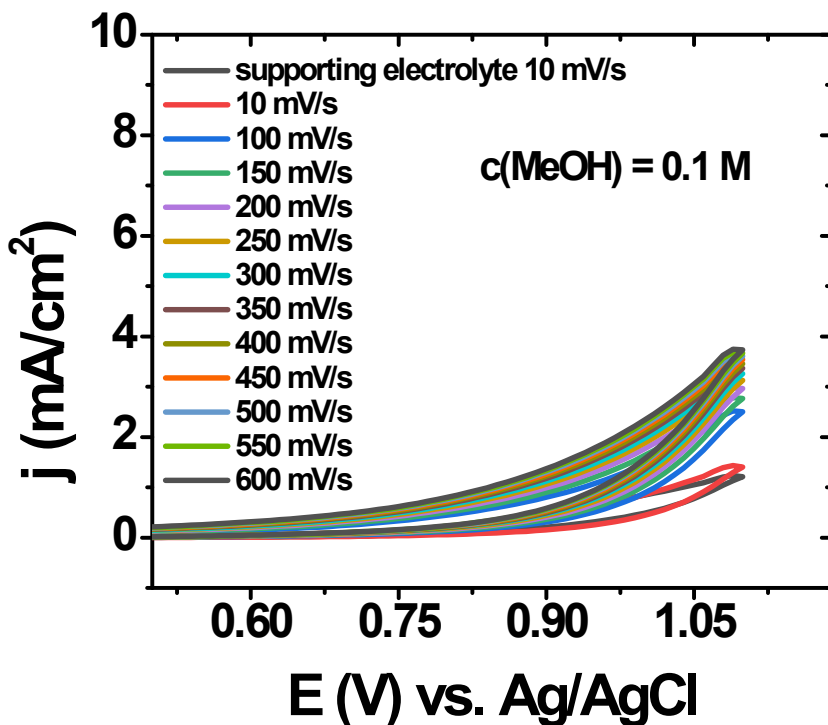


Figure S4. Cyclic voltammetry at different scan rates of glassy carbon electrodes modified with the $\text{La}_{0.88}\text{Fe}_{0.93}\text{Cu}_{0.05}\text{Pd}_{0.02}\text{O}_3$ perovskite and $c(\text{methanol}) = 0.1 \text{ M}$ dissolved in $\text{NaOH} = 1 \text{ M}$.

This Supplementary Information replaces the original version published on 16 January 2026. The files previously available on the platform are now accessible from the repository at <https://zenodo.org/records/18154388>.

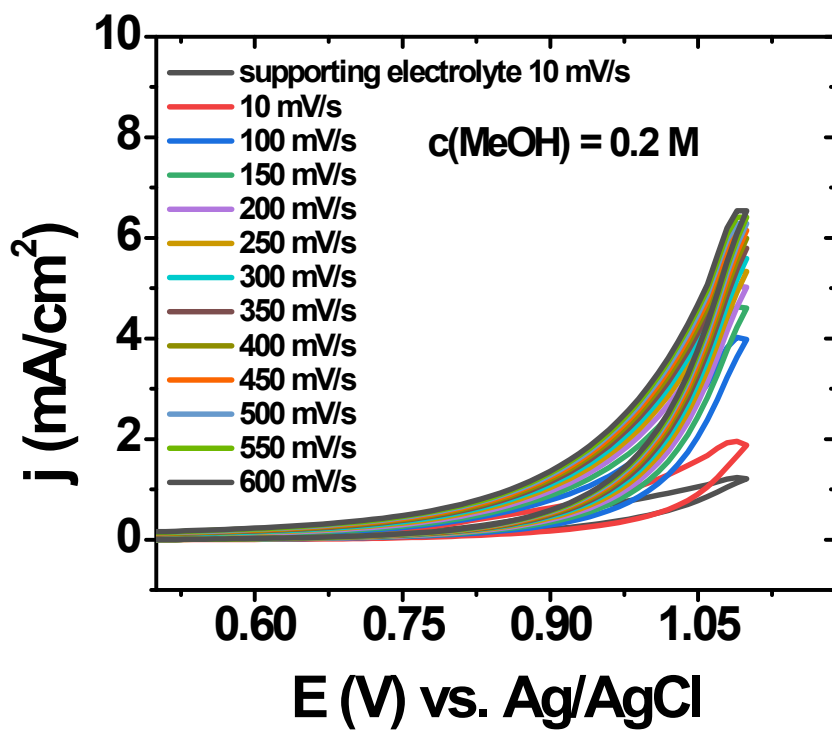


Figure S5. Cyclic voltammetry at different scan rates of glassy carbon electrodes modified with the $\text{La}_{0.88}\text{Fe}_{0.93}\text{Cu}_{0.05}\text{Pd}_{0.02}\text{O}_3$ perovskite and $c(\text{methanol}) = 0.2 \text{ M}$ dissolved in $\text{NaOH} = 1 \text{ M}$.

This Supplementary Information replaces the original version published on 16 January 2026. The files previously available on the platform are now accessible from the repository at <https://zenodo.org/records/18154388>.

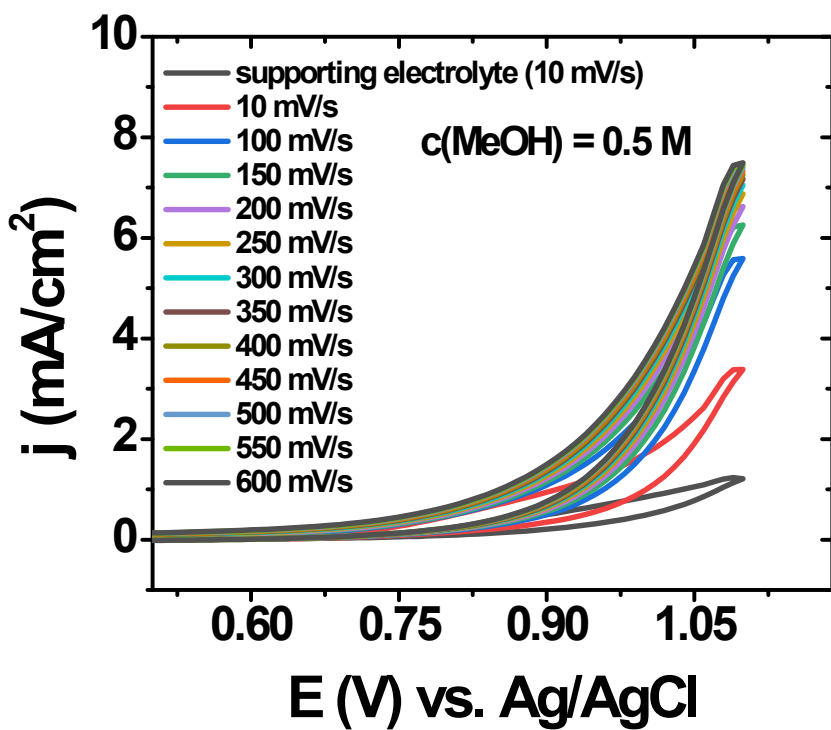


Figure S6. Cyclic voltammetry at different scan rates of glassy carbon electrodes modified with the $\text{La}_{0.88}\text{Fe}_{0.93}\text{Cu}_{0.05}\text{Pd}_{0.02}\text{O}_3$ perovskite and $c(\text{methanol}) = 0.5 \text{ M}$ dissolved in $\text{NaOH} = 1 \text{ M}$.

This Supplementary Information replaces the original version published on 16 January 2026. The files previously available on the platform are now accessible from the repository at <https://zenodo.org/records/18154388>.

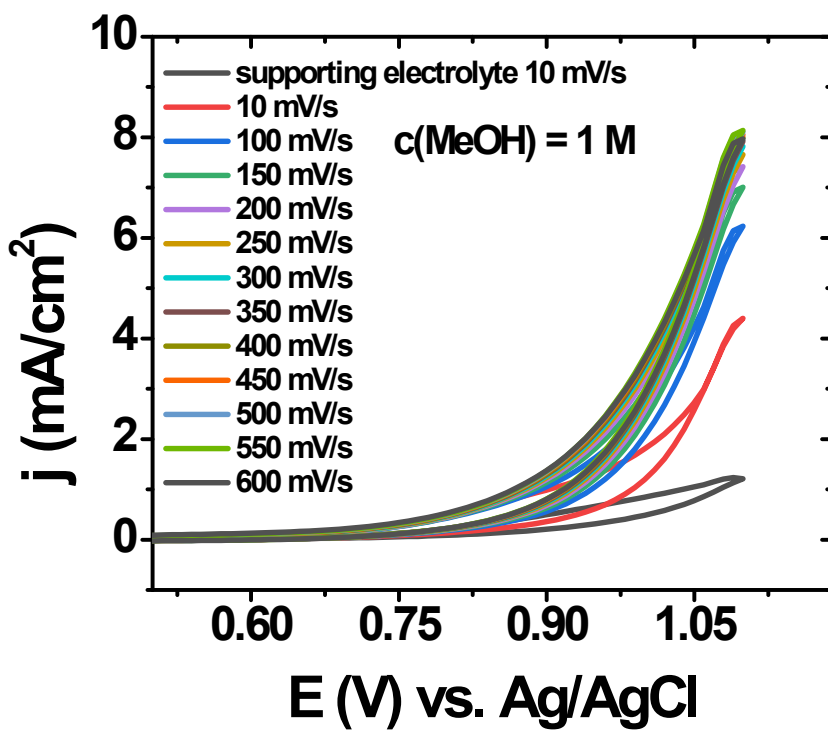


Figure S7. Cyclic voltammetry at different scan rates of glassy carbon electrodes modified with the $\text{La}_{0.88}\text{Fe}_{0.93}\text{Cu}_{0.05}\text{Pd}_{0.02}\text{O}_3$ perovskite and $c(\text{methanol}) = 1 \text{ M}$ dissolved in $\text{NaOH} = 1 \text{ M}$.

This Supplementary Information replaces the original version published on 16 January 2026. The files previously available on the platform are now accessible from the repository at <https://zenodo.org/records/18154388>.

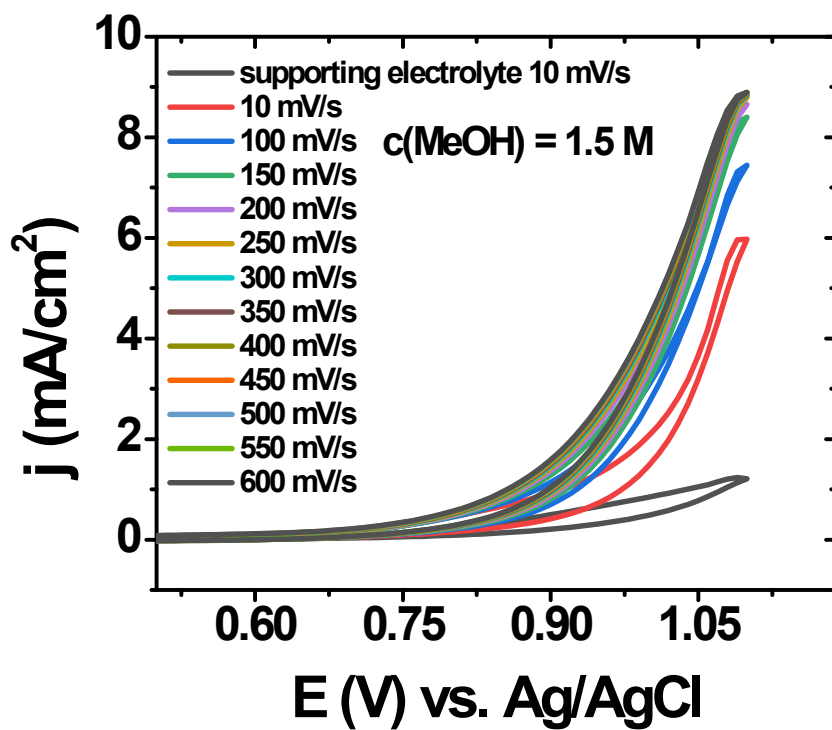


Figure S8. Cyclic voltammetry at different scan rates of glassy carbon electrodes modified with the $\text{La}_{0.88}\text{Fe}_{0.93}\text{Cu}_{0.05}\text{Pd}_{0.02}\text{O}_3$ perovskite and $c(\text{methanol}) = 1.5 \text{ M}$ dissolved in $\text{NaOH} = 1 \text{ M}$.

This Supplementary Information replaces the original version published on 16 January 2026. The files previously available on the platform are now accessible from the repository at <https://zenodo.org/records/18154388>.

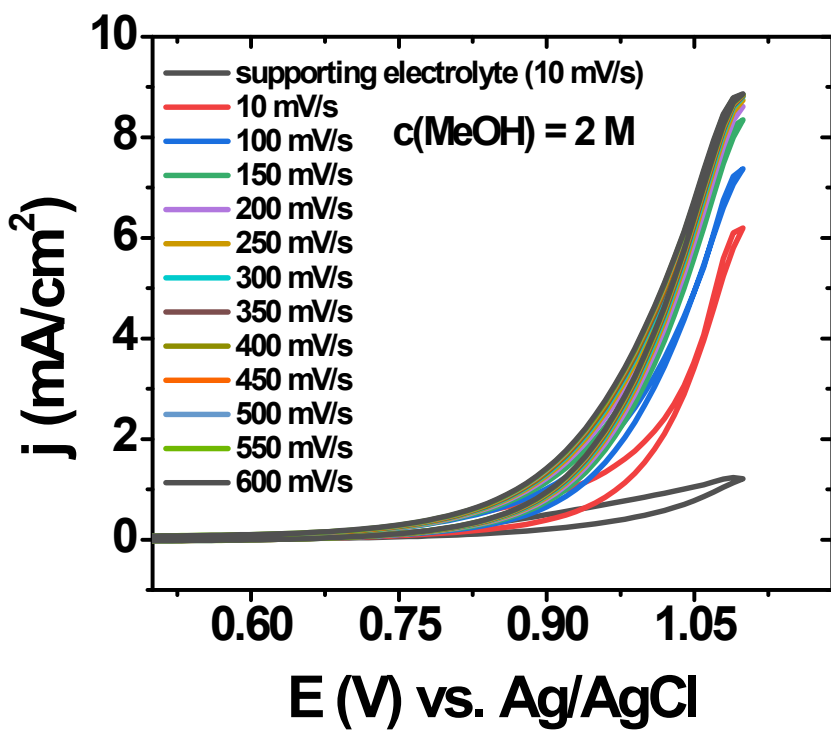


Figure S9. Cyclic voltammetry at different scan rates of glassy carbon electrodes modified with the $\text{La}_{0.88}\text{Fe}_{0.93}\text{Cu}_{0.05}\text{Pd}_{0.02}\text{O}_3$ perovskite and $c(\text{methanol}) = 2 \text{ M}$ dissolved in $\text{NaOH} = 1 \text{ M}$.

This Supplementary Information replaces the original version published on 16 January 2026. The files previously available on the platform are now accessible from the repository at <https://zenodo.org/records/18154388>.

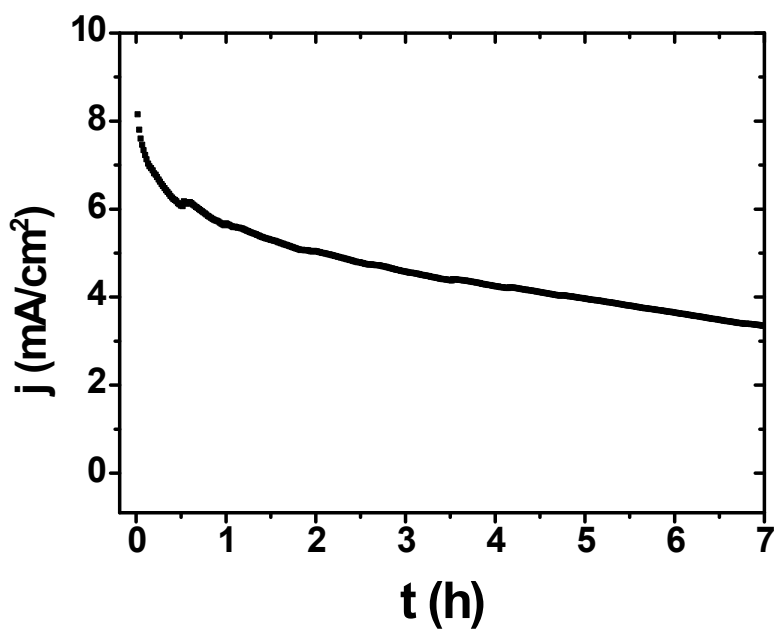


Figure S10. Chronoamperometric trace of methanol electrooxidation for the GCE|La_{0.88}Fe_{0.93}Cu_{0.05}Pd_{0.02}O₃|Nafion system; c(MeOH) = 2 M, c(NaOH) = 1 M, c(Na₂SO₄) = 0.1 M.

This Supplementary Information replaces the original version published on 16 January 2026. The files previously available on the platform are now accessible from the repository at <https://zenodo.org/records/18154388>.

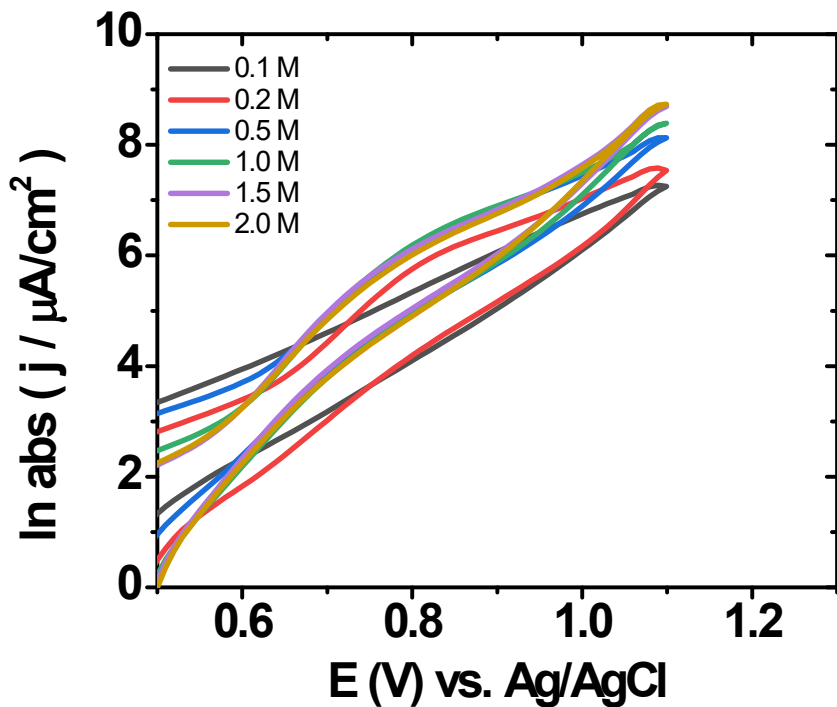


Figure S11. Tafel plot recorded at 10 mV/s of glassy carbon electrodes modified with the $\text{La}_{0.88}\text{Fe}_{0.93}\text{Cu}_{0.05}\text{Pd}_{0.02}\text{O}_3$ perovskite at different concentrations of methanol, as expressed by the legend in the upper left.

This Supplementary Information replaces the original version published on 16 January 2026. The files previously available on the platform are now accessible from the repository at <https://zenodo.org/records/18154388>.

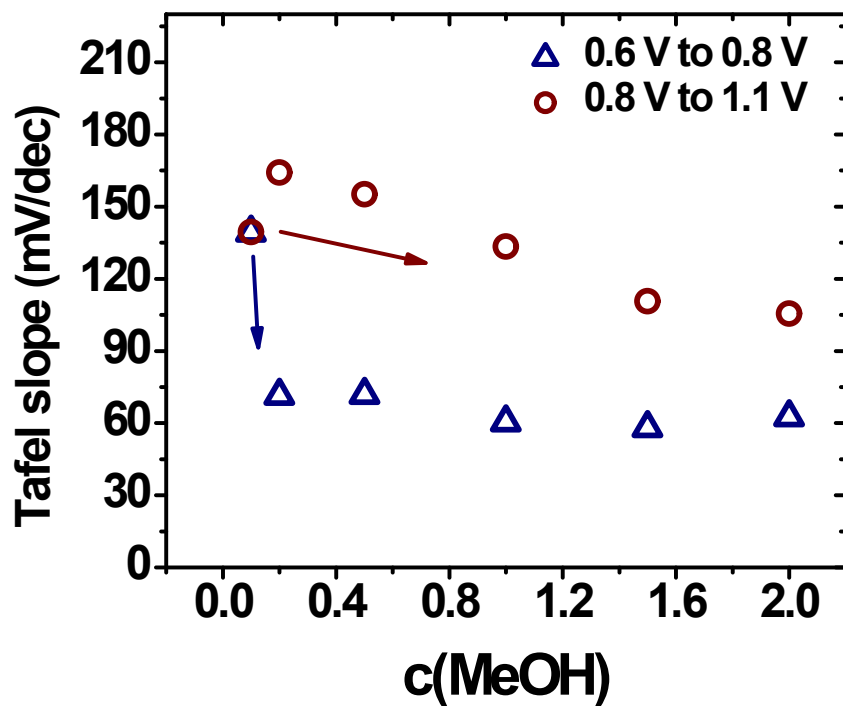


Figure S12. Tafel slope determined from Figure S7 in different potential windows for the GCE|La_{0.88}Fe_{0.93}Cu_{0.05}Pd_{0.02}O₃|Nafion system.

This Supplementary Information replaces the original version published on 16 January 2026. The files previously available on the platform are now accessible from the repository at <https://zenodo.org/records/18154388>.

8. Operando EC-Raman measurements

Spectro-electrochemical measurements were performed using an EC-Raman cell designed by HORIBA (figure below), with an active surface area of 0.79 cm^2 and equipped with a fluidic system. During the experiments, the flow rate inside the cell was fixed at $60 \text{ mL} \cdot \text{min}^{-1}$ to ensure efficient bubble removal.

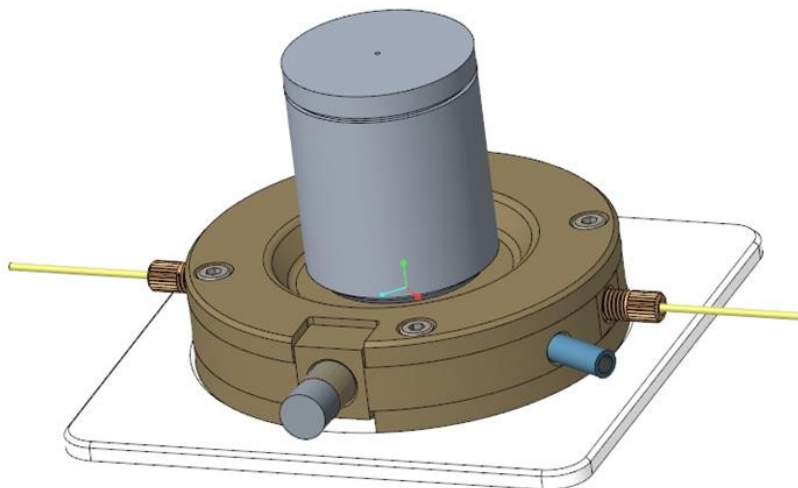


Figure S13. 3D representation of the HORIBA EC-Raman Cell

Potentiostatic electrochemical measurements (chronoamperometry and chronopotentiometry) were performed using a BioLogic SP-150e potentiostat during simultaneous Raman acquisition, with data recorded and processed via EC-Lab software.

Raman spectra were collected using a LabRAM Soleil microspectrometer (HORIBA France SAS) equipped with a 532 nm laser (maximum power 108 mW) and an 1800 grooves/mm diffraction grating. The acquisition and processing of the spectroscopic data (Raman spectra with fluorescence background) were carried out using LabSpec software.

For powder analysis, the laser power was limited to 3.5 mW to avoid laser-induced degradation. Spectra were acquired using a Nikon 50× long working distance objective (numerical aperture = 0.6), with an integration time of 10 s and 15 accumulations per spectrum.

For Operando EC-Raman measurements, the laser power was set to 54 mW. The sapphire window of the EC-Raman cell provides a transmission of approximately 85% over the relevant spectral range. Each spectrum was recorded with an integration time of 8 s and 10 accumulations. All measurements were performed using a $10 \times 10 \mu\text{m}$ macrospot generated by HORIBA's patented QScan technology, ensuring uniform illumination without loss of laser intensity or confocality.

This Supplementary Information replaces the original version published on 16 January 2026. The files previously available on the platform are now accessible from the repository at <https://zenodo.org/records/18154388>.

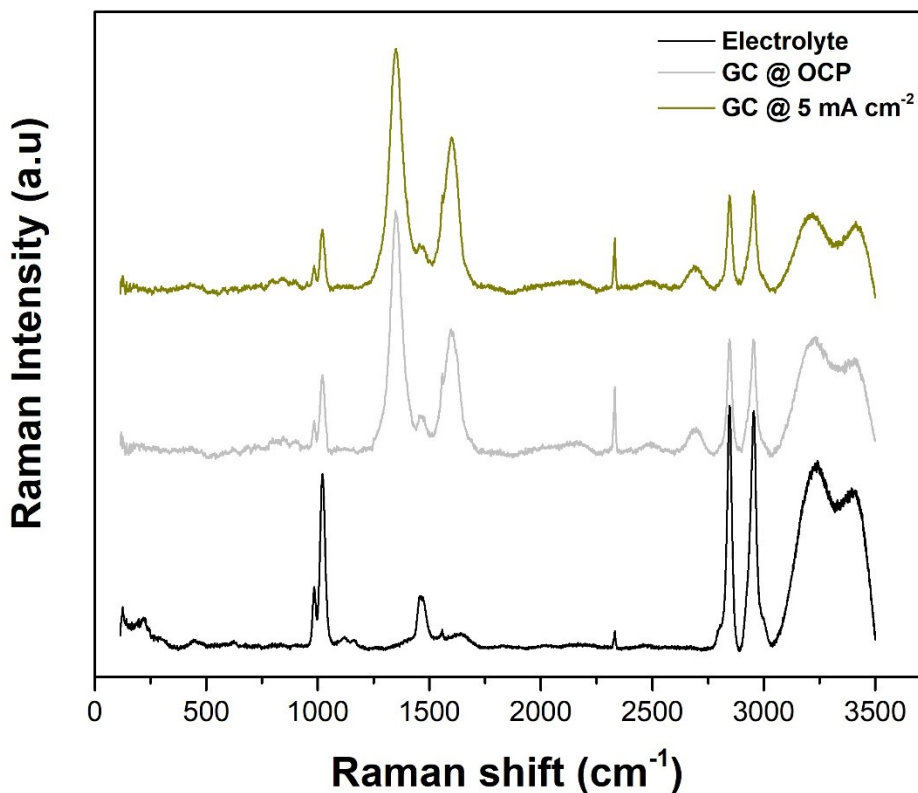


Figure S14. *Operando* Raman spectra of bare glassy carbon in alkaline media (1 M NaOH) containing 0.1 M Na₂SO₄ and 2 M MeOH, recorded at open circuit potential (OCP) and under an applied current density of 5 mA cm⁻², along with the Raman spectrum of the same electrolyte measured in a cuvette.

This Supplementary Information replaces the original version published on 16 January 2026. The files previously available on the platform are now accessible from the repository at <https://zenodo.org/records/18154388>.

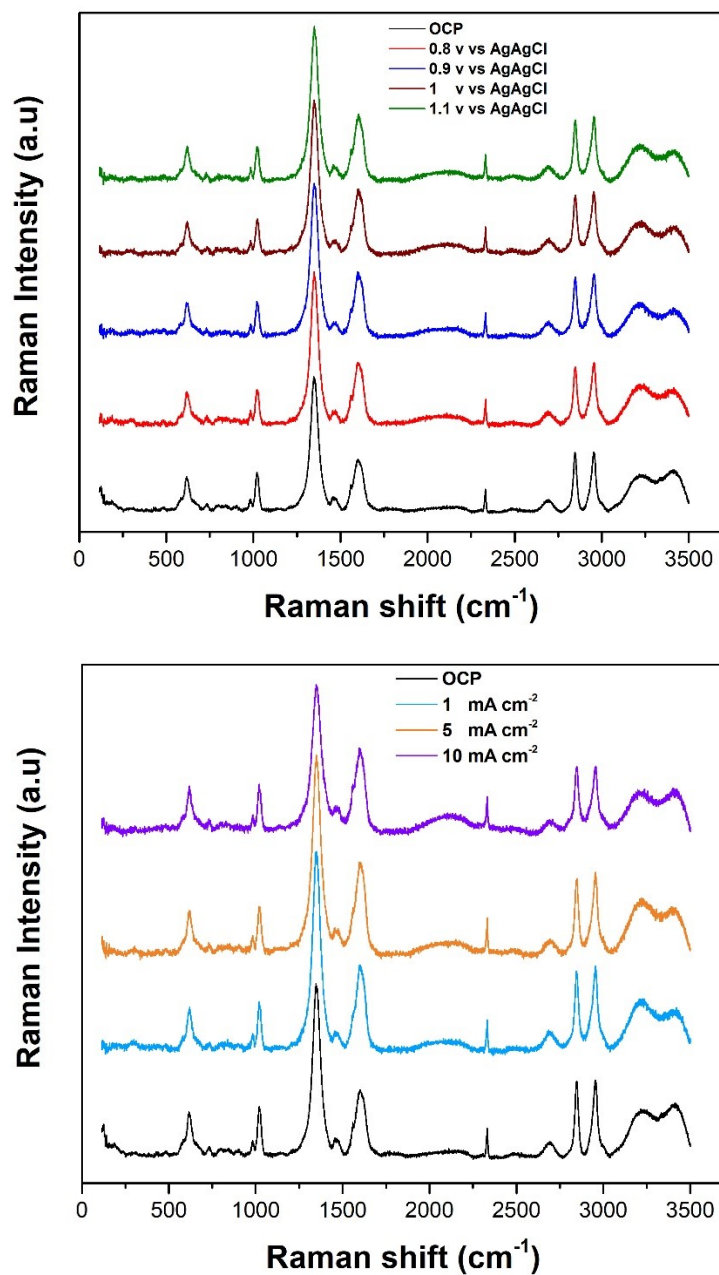


Figure S15. *Operando* Raman spectra of a 10 μL drop of a mixture of $\text{La}_{0.88}\text{Fe}_{0.93}\text{Cu}_{0.05}\text{Pd}_{0.02}\text{O}_3$ and Nafion deposited on the electrode surface, recorded during chronoamperometry (top) and chronopotentiometry (bottom).

This Supplementary Information replaces the original version published on 16 January 2026. The files previously available on the platform are now accessible from the repository at <https://zenodo.org/records/18154388>.

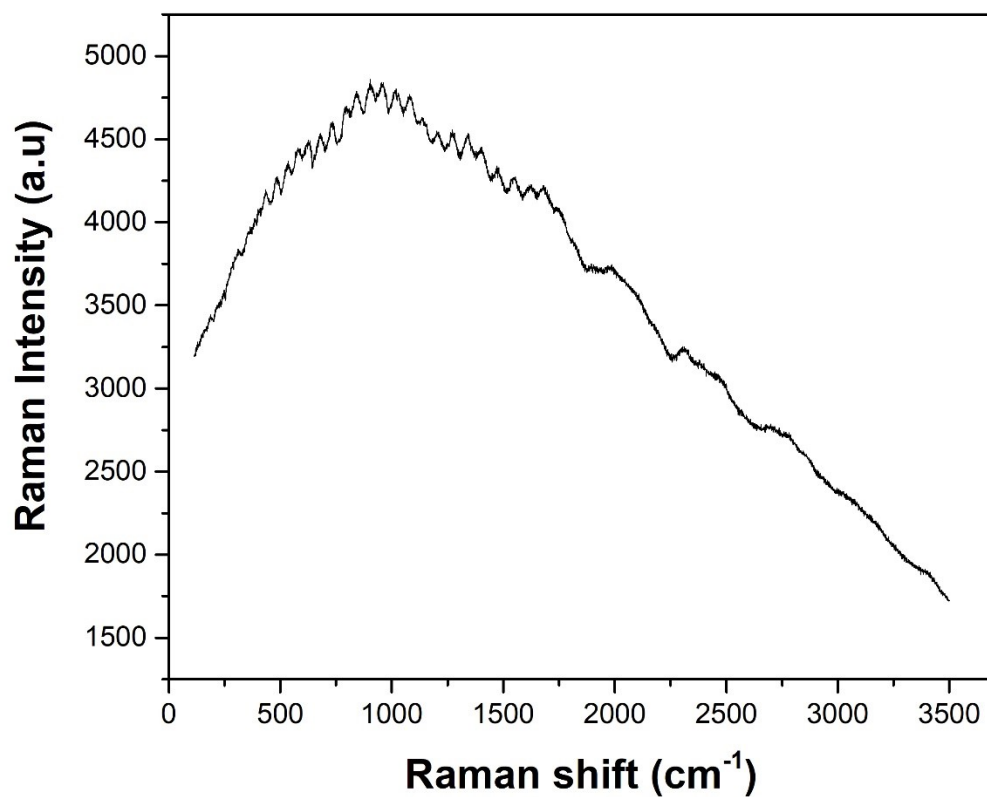


Figure S16. Raman spectra showing a strong fluorescence background from Nafion, obtained from three 10 μ L drops dried on gold surface and recorded using a 532 nm laser with an intensity of 100 μ W.

This Supplementary Information replaces the original version published on 16 January 2026. The files previously available on the platform are now accessible from the repository at <https://zenodo.org/records/18154388>.

9. Additional results from DFT

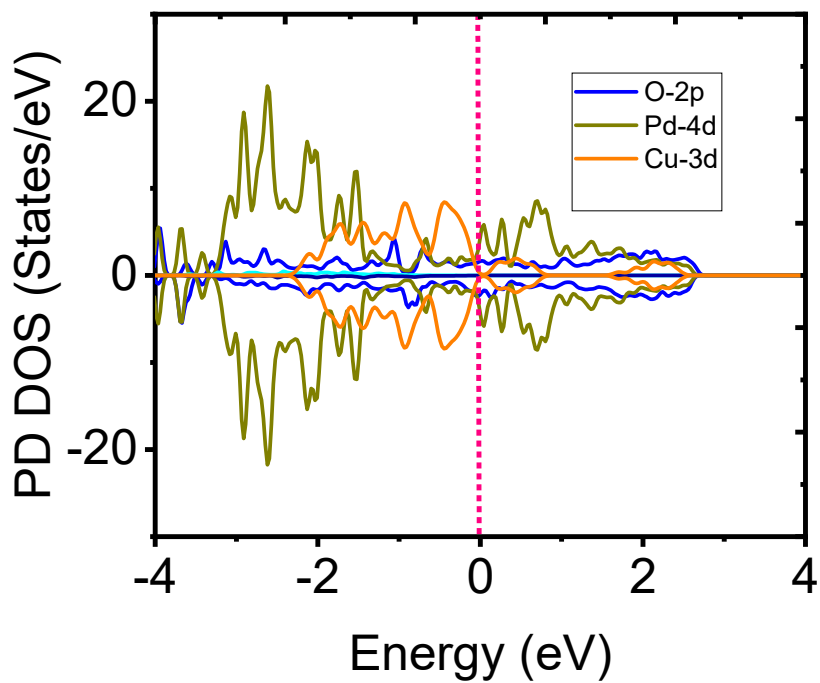


Figure S17. PD-DOS states for O-2p, Pd-4d and Cu-3d.

This Supplementary Information replaces the original version published on 16 January 2026. The files previously available on the platform are now accessible from the repository at <https://zenodo.org/records/18154388>.

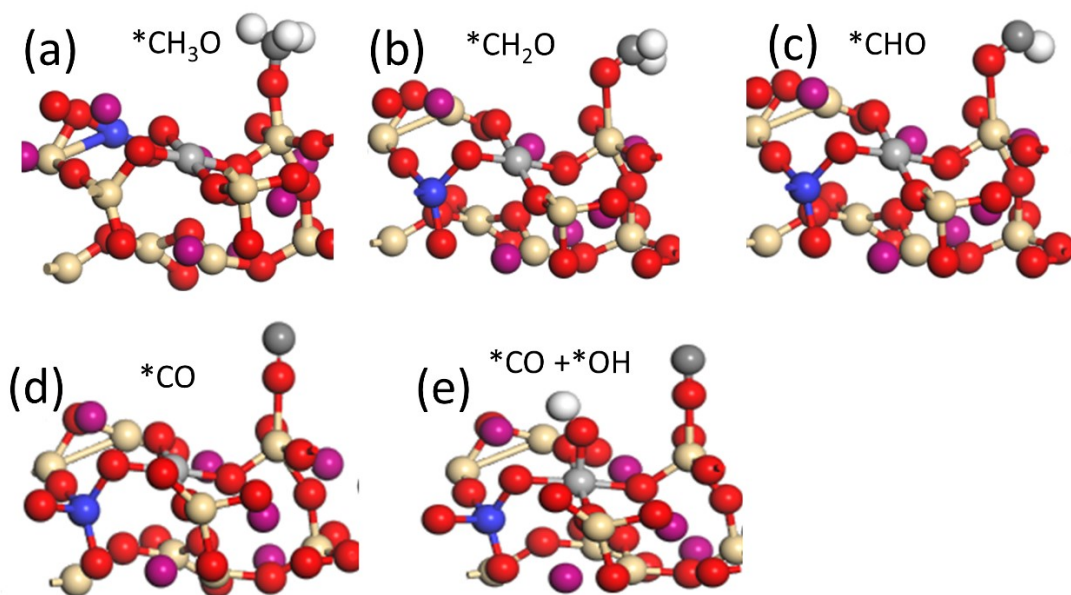


Figure S18. Structural motifs of the different reaction intermediates calculated for the methanol oxidation reaction.

This Supplementary Information replaces the original version published on 16 January 2026. The files previously available on the platform are now accessible from the repository at <https://zenodo.org/records/18154388>.

10. Determination of the electroactive area of the modified electrode

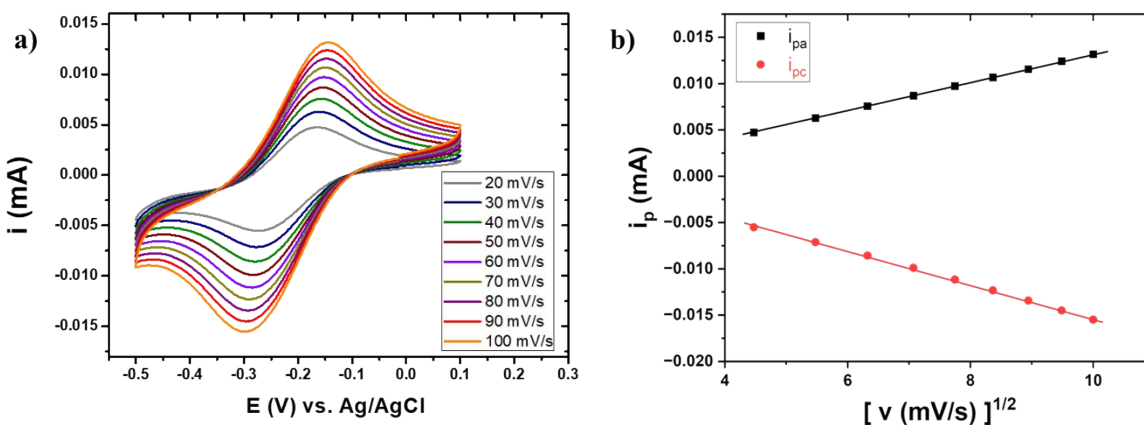


Figure S19. Determination of the electroactive surface area of a of the GCE modified with $\text{La}_{0.88}\text{Fe}_{0.93}\text{Cu}_{0.05}\text{Pd}_{0.02}\text{O}_3|\text{Nafion}$; (a) cyclic voltammograms for a solution consisting in $\text{Ru}(\text{NH}_3)_6\text{Cl}_3$ $5 \cdot 10^{-4}$ mol/mL in Na_2SO_4 0.1 mol/L; $D[\text{Ru}(\text{NH}_3)_6\text{Cl}_3] = 8.43 \cdot 10^{-6}$ cm^2/s [29], (b) linear relation between the peak current and the square of the scan rate.

The electroactive area of the $\text{GCE}|\text{La}_{0.88}\text{Fe}_{0.93}\text{Cu}_{0.05}\text{Pd}_{0.02}\text{O}_3|\text{Nafion}$ system was determined using the Randles-Ševčík equation [30], which takes for the form of equation S11 at 25 °C for A expressed in cm^2 , D in cm^2/s , c in mol/mL, v in V/s and i_p in Ampères.

$$i_p = (2.69 \cdot 10^5) n^{3/2} A D^{1/2} c v^{1/2} \quad (\text{S11})$$

This Supplementary Information replaces the original version published on 16 January 2026. The files previously available on the platform are now accessible from the repository at <https://zenodo.org/records/18154388>.

References

- [1] A. et al. Grimaud, Double perovskites as a family of highly active catalysts for oxygen evolution in alkaline solution, *Nat. Comm.* 4 (2013) 4239.
- [2] H. Shi, G. Zhao, Water oxidation on spinel NiCo₂O₄ nanoneedles anode: microstructures, specific surface character, and the enhanced electrocatalytic performance, *J. Phys. Chem. C* 118 (2014) 25939.
- [3] J.O. Bockris, T. Otagawat, Mechanism of Oxygen Evolution on Perovskites, *J. Phys. Chem* 87 (1983) 2960–2971. <https://doi.org/10.1021/j100238a048>.
- [4] Z. Zhang, J. Liu, J. Wang, Q. Wang, Y. Wang, K. Wang, Z. Wang, M. Gu, Z. Tang, J. Lim, T. Zhao, F. Ciucci, Single-atom catalyst for high-performance methanol oxidation, *Nat. Commun.* 12 (2021) 5235. <https://doi.org/10.1038/s41467-021-25562-y>.
- [5] Y. Liu, Y. Zhang, X. Tian, H. Wang, L. Huo, Ultra-high activity methanol oxidation electrocatalyzed by a flexible integrated Pt-Zn array electrode, *J. Mater. Chem. C* 13 (2025) 3054–3061. <https://doi.org/10.1039/d4tc04584j>.
- [6] T. Liu, Q.X. Chen, Z. He, J.L. Wang, S.Z. Sheng, J.W. Liu, S.H. Yu, Efficient Methanol Oxidation Kinetics Enabled by an Ordered Heterocatalyst with Dual Electric Fields, *J. Am. Chem. Soc.* 147 (2025) 5340–5349. <https://doi.org/10.1021/jacs.4c16885>.
- [7] L. Hui, Y. Xue, C. Xing, Y. Liu, Y. Du, Y. Fang, H. Yu, C. Zhang, F. He, Y. Li, Atomic alloys of nickel-platinum on carbon network for methanol oxidation, *Nano Energy* 95 (2022) 106984. <https://doi.org/10.1016/j.nanoen.2022.106984>.
- [8] R. Ganesan, D.J. Ham, J.S. Lee, Platinized mesoporous tungsten carbide for electrochemical methanol oxidation, *Electrochem. Commun.* 9 (2007) 2576–2579. <https://doi.org/10.1016/j.elecom.2007.08.002>.
- [9] S.M. Alia, G. Zhang, D. Kisailus, D. Li, S. Gu, K. Jensen, Y. Yan, Porous platinum nanotubes for oxygen reduction and methanol oxidation reactions, *Adv. Funct. Mater.* 20 (2010) 3742–3746. <https://doi.org/10.1002/adfm.201001035>.
- [10] F. Luo, Y. Yu, X. Long, C. Li, T. Xiong, Z. Yang, Boosting catalytic activity toward methanol oxidation reaction for platinum via heterostructure engineering, *J. Colloid Interface Sci.* 656 (2024) 450–456. <https://doi.org/10.1016/j.jcis.2023.11.077>.
- [11] B. Narayanamoorthy, K.K.R. Datta, M. Eswaramoorthy, S. Balaji, Highly active and stable Pt₃Rh nanoclusters as supportless electrocatalyst for methanol oxidation in direct methanol fuel cells, *ACS Catal.* 4 (2014) 3621–3629. <https://doi.org/10.1021/cs500628m>.

This Supplementary Information replaces the original version published on 16 January 2026. The files previously available on the platform are now accessible from the repository at <https://zenodo.org/records/18154388>.

- [12] H. Xu, D.J. Zheng, H. Iriawan, J.H. Fang, J. Kim, X. Wang, Y. Román-Leshkov, J. Li, Y. Shao-Horn, A Cobalt-Platinum-Ruthenium System for Acidic Methanol Oxidation, *Chem. Mater.* 36 (2024) 6938–6949. <https://doi.org/10.1021/acs.chemmater.4c01008>.
- [13] H. You, F. Zhang, Z. Liu, J. Fang, Free-standing Pt-Au hollow nanourchins with enhanced activity and stability for catalytic methanol oxidation, *ACS Catal.* 4 (2014) 2829–2835. <https://doi.org/10.1021/cs500390s>.
- [14] X. Wang, W. Wang, Z. Qi, C. Zhao, H. Ji, Z. Zhang, High catalytic activity of ultrafine nanoporous palladium for electro-oxidation of methanol, ethanol, and formic acid, *Electrochem. Commun.* 11 (2009) 1896–1899. <https://doi.org/10.1016/j.elecom.2009.08.011>.
- [15] J. Li, C. Wang, H. Shang, Y. Wang, H. You, H. Xu, Y. Du, Metal-modified PtTe₂ nanorods: Surface reconstruction for efficient methanol oxidation electrocatalysis, *Chem. Eng. J.* 424 (2021) 130319. <https://doi.org/10.1016/j.cej.2021.130319>.
- [16] C.F. Tsai, K.Y. Yeh, P.W. Wu, Y.F. Hsieh, P. Lin, Effect of platinum present in multi-element nanoparticles on methanol oxidation, *J. Alloys Compd.* 478 (2009) 868–871. <https://doi.org/10.1016/j.jallcom.2008.12.055>.
- [17] Z. Li, X. Jiang, X. Wang, J. Hu, Y. Liu, G. Fu, Y. Tang, Concave PtCo nanocrosses for methanol oxidation reaction, *Appl. Catal. B Environ.* 277 (2020) 119135. <https://doi.org/10.1016/j.apcatb.2020.119135>.
- [18] S. Xue, W. Deng, F. Yang, J. Yang, I.S. Amiinu, D. He, H. Tang, S. Mu, Hexapod PtRuCu Nanocrystalline Alloy for Highly Efficient and Stable Methanol Oxidation, *ACS Catal.* 8 (2018) 7578–7584. <https://doi.org/10.1021/acscatal.8b00366>.
- [19] R. Ojani, E. Hasheminejad, J.B. Raoof, Direct growth of 3D flower-like Pt nanostructures by a template-free electrochemical route as an efficient electrocatalyst for methanol oxidation reaction, *Energy* 90 (2015) 1122–1131. <https://doi.org/10.1016/j.energy.2015.06.061>.
- [20] C.K. Poh, Z. Tian, J. Gao, Z. Liu, J. Lin, Y.P. Feng, F. Su, Nanostructured trimetallic Pt/FeRuC, Pt/NiRuC, and Pt/CoRuC catalysts for methanol electrooxidation, *J. Mater. Chem.* 22 (2012) 13643–13652. <https://doi.org/10.1039/c2jm31956j>.
- [21] Y. Wang, Z. Li, X. Zheng, R. Wu, J. Song, Y. Chen, X. Cao, Y. Nie, Renovating phase constitution and construction of Pt nanocubes for electrocatalysis of methanol oxidation via a solvothermal-induced strong metal-support interaction, *Appl. Catal. B Environ.* 325 (2023) 122383. <https://doi.org/10.1016/j.apcatb.2023.122383>.
- [22] Y.W. Lee, J.Y. Lee, D.H. Kwak, E.T. Hwang, J.I. Sohn, K.W. Park, Pd@Pt core-shell nanostructures for improved electrocatalytic activity in methanol oxidation reaction, *Appl. Catal. B Environ.* 179 (2015) 178–184. <https://doi.org/10.1016/j.apcatb.2015.05.029>.

This Supplementary Information replaces the original version published on 16 January 2026. The files previously available on the platform are now accessible from the repository at <https://zenodo.org/records/18154388>.

- [23] K. Mandal, D. Bhattacharjee, P.S. Roy, S.K. Bhattacharya, S. Dasgupta, Room temperature synthesis of Pd-Cu nanoalloy catalyst with enhanced electrocatalytic activity for the methanol oxidation reaction, *Appl. Catal. A Gen.* 492 (2015) 100–106. <https://doi.org/10.1016/j.apcata.2014.12.012>.
- [24] T. Jurzinsky, C. Cremers, K. Pinkwart, J. Tübke, On the Influence of Ag on Pd-based Electrocatalyst for Methanol Oxidation in Alkaline Media: A Comparative Differential Electrochemical Mass Spectrometry Study, *Electrochim. Acta* 199 (2016) 270–279. <https://doi.org/10.1016/j.electacta.2016.01.172>.
- [25] I.-M. Hsing, X. Wang, Y.-J. Leng, Electrochemical Impedance Studies of Methanol Electro-oxidation on Pt/C Thin Film Electrode, *J. Electrochem. Soc.* 149 (2002) A615. <https://doi.org/10.1149/1.1467940>.
- [26] S. Shahrokhian, S. Rezaee, Vertically standing Cu₂O nanosheets promoted flower-like PtPd nanostructures supported on reduced graphene oxide for methanol electro-oxidation, *Electrochim. Acta* 259 (2018) 36–47. <https://doi.org/10.1016/j.electacta.2017.10.141>.
- [27] D.J. Chen, Y.J. Tong, Irrelevance of Carbon Monoxide Poisoning in the Methanol Oxidation Reaction on a PtRu Electrocatalyst, *Angew. Chemie - Int. Ed.* 54 (2015) 9394–9398. <https://doi.org/10.1002/anie.201503917>.
- [28] J.O. Bockris, A.K.N. Reddy, M. Gamboa-Aldeco, Rate-Determining Steps and Energy Barriers for Multistep Reactions, in: *Mod. Electrochem. Vol. 2A; Fundam. Electrochem.*, 2nd ed., Kluwer Academic Publishers, New York, 2002: pp. 1180–1187.
- [29] Y. Wang, J.G. Limon-Petersen, R.G. Compton, Measurement of the diffusion coefficients of [Ru(NH₃)₆]³⁺ and [Ru(NH₃)₆]²⁺ in aqueous solution using microelectrode double potential step chronoamperometry, *J. Electroanal. Chem.* 652 (2011) 13–17. <https://doi.org/10.1016/j.jelechem.2010.12.011>.
- [30] A.J. Bard, L.R. Faulkner, *Electrochemical Methods Fundamentals and Applications*, 2nd ed., John Wiley & Sons, Inc., 2001.